Variability of Zonal Mean Tropical Temperatures Derived from a Decade of GPS Radio Occultation Data

WILLIAM J. RANDEL AND FEI WU

National Center for Atmospheric Research, Boulder, Colorado*

(Manuscript received 25 July 2014, in final form 30 October 2014)

ABSTRACT

Variability in tropical zonal mean temperatures over 10–30 km is analyzed based on high-quality, high-vertical-resolution GPS temperature measurements covering 2001–13. The observations are used to quantify variability spanning time scales of weeks to over a decade, with focus on behavior of the tropopause region and coupling with the upper troposphere and stratosphere. Large variations associated with the seasonal cycle, quasi-biennial oscillation (QBO), and El Niño–Southern Oscillation (ENSO) are isolated and removed, and residual time series are analyzed using principal components and spectrum analysis. The residual temperature exhibits maximum variance in the lower stratosphere, with a vertical structure similar to the seasonal cycle. Residual temperatures exhibit two dominant modes of variability: a ''deep stratosphere mode'' tied to high-latitude planetary wave forcing and a shallow ''near-tropopause mode'' linked to dynamically forced upwelling near the tropopause. Variations in the cold point tropopause (and by inference in global stratospheric water vapor) are closely tied to the near-tropopause mode. These coherent temperature patterns provide further evidence of distinct upper and lower branches of the tropical Brewer–Dobson circulation. Zonal mean temperatures in the lower stratosphere and near the cold point are most strongly coupled to the upper troposphere on time scales of ~(30–60) days, probably linked to the Madden–Julian oscillation (MJO). Enhanced temperature variance near the tropopause is consistent with the long radiative relaxation time scales in the lower stratosphere, which makes this region especially sensitive to low-frequency dynamical forcing.

1. Introduction

The thermal structure and variability in the tropics are fundamental to many aspects of the climate system. Large-scale tropospheric temperatures in the tropics are characterized by a small annual cycle but large interannual changes linked to the El Niño–Southern Oscillation (ENSO; Yulaeva and Wallace 1994). In contrast, tropical stratospheric temperatures exhibit a distinct annual cycle (focused in the lower stratosphere), along with large interannual variations linked to the quasi-biennial oscillation (QBO). The tropical stratosphere is also influenced by forcing from extratropical planetary waves (Randel 1993; Yulaeva et al. 1994; Ueyama and Wallace 2010; Ueyama et al. 2013; Grise and Thompson 2013) together with ENSO (Randel et al. 2009). The tropical cold point tropopause is of special importance, as it is closely linked to variations in global stratospheric water vapor (Mote et al. 1996; Randel and Jensen 2013; Fueglistaler et al. 2013) and tropical cirrus clouds (Davis et al. 2013; Li and Thompson 2013). However, fundamental behavior of the cold point tropical tropopause and its links to tropospheric and stratospheric circulation is not well understood from either a theoretical or observational basis; for example, interannual variability and trends in cold point temperatures show significant differences among different observational datasets (Wang et al. 2012) and also between data and models (Kim et al. 2013). An additional complication is that the tropopause region and cold point are characterized by narrow vertical-scale features, which are not well resolved in either nadir sounding satellite measurements (e.g., Microwave Sounding Unit) or meteorological analysis or reanalysis data (with typical vertical resolutions of 1 km or greater).

Our objective in the present study is to utilize a long record of high-quality, high-vertical-resolution global

* The National Center for Atmospheric Research is sponsored by the National Science Foundation.

Corresponding author address: William Randel, Atmospheric Chemistry Division, National Center for Atmospheric Research, 3450 Mitchell Lane, Boulder, CO 80301.
E-mail: randel@ucar.edu

DOI: 10.1175/JAS-D-14-0216.1

positioning system (GPS) radio occultation temperature measurements to characterize thermal variability of the tropics and coupling between the troposphere, tropopause region, and stratosphere. We focus on variability of the zonal mean temperature because 1) the zonal mean is highly constrained by GPS measurements and 2) zonal means can be analyzed and understood based on a relatively simple theoretical framework. The zonal mean thermodynamic equation [in transformed Eulerian mean (TEM) coordinates; Andrews et al. 1987] is

$$\overline{T}_t = -\overline{v}^*\overline{T}_y - \overline{w}^* S + \overline{Q} - e^{z/H}\left[e^{-z/H}\left(\overline{v'T'}\frac{\overline{T}_y}{S} + \overline{w'T'}\right)\right]_z \quad (1)$$

Here $\overline{T}$ is zonally averaged temperature, ($\overline{v}^*$, $\overline{w}^*$) are components of the residual meridional circulation, S is a stability parameter, and $\overline{Q}$ is the zonal mean diabatic heating. The eddy terms in (1) are generally small (although not negligible near the tropical tropopause; Abalos et al. 2013), and the $\overline{v}^*$ term is also small in the deep tropics, so that the approximate thermodynamic balance is

$$\overline{T}_t = -\overline{w}^* S + \overline{Q}. \quad (2)$$

In the troposphere, $\overline{Q}$ is mainly linked to large-scale convective heating and radiative cooling, while in the stratosphere radiation is dominant [and $\overline{Q}$ is often approximated by a relaxation of the form $\overline{Q} = -\alpha(\overline{T} - \overline{T}_{eq})$, with $\overline{T}_{eq}$ a background equilibrium temperature and α an inverse radiative damping time scale; e.g., Andrews et al. 1987; Hitchcock et al. 2010]. Hence, zonal mean temperatures in the tropical tropopause region and above can be primarily understood in terms of (dynamically forced) upwelling $\overline{w}^*$ and the response to radiative effects. Note that the latter can include the radiative influence of temporally and spatially varying constituents, especially ozone (Fueglistaler et al. 2011). The controlling influence of upwelling on tropical temperature is confirmed by analysis of meteorological datasets and model simulations (Abalos et al. 2012, 2013).

This study will focus on the observed variability of zonal mean temperatures from GPS data spanning June 2001–September 2013. While daily data are available for much of the record, we focus on the analysis of pentad (5-day average) data because we are most interested in variability for periods of weeks to years (and there is relatively little observed variance of zonal means on shorter time scales). We isolate and remove the mean annual cycle, together with the well-known QBO and ENSO effects (via linear regression), in order to focus on understanding residual variability (which is relatively large, especially in the tropopause region). Our analysis of zonal mean variability is a complement to studies of the local (latitude–longitude dependent) cold point tropopause structure and variability (e.g., Kim and Son 2012; Munchak and Pan 2014), which is dominated by various tropical waves. We also complement the study of Grise and Thompson (2013), who focused on a shorter record of GPS temperatures and statistical links to tropical and extratropical forcings.

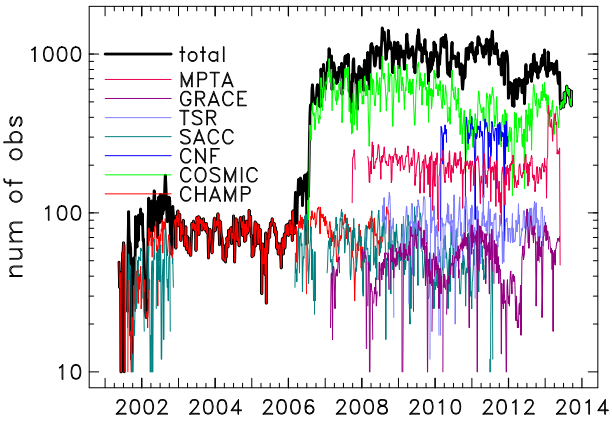

FIG. 1. Number of GPS observations for 5-day averages (pentads) in the latitude band 10°N–10°S from the separate satellite measurements (colors), together with the total (black). Note the logarithmic vertical axis.

2. Data and analysis

a. GPS data

We analyze zonal mean temperatures derived from GPS measurements covering 2001–13. GPS data have the attributes of high quality and high vertical resolution (<1 km) over ~(10–30) km, with near-global sampling (e.g., Anthes et al. 2008). We include and combine data from seven individual satellites (or constellations, in the case of COSMIC), including *CHAMP*, Satelite de Aplicaciones Cientificas-C (SACC), COSMIC, GRACE, *TerraSAR-X* (TSX), Communications/Navigation Outage Forecasting System (CNOFS) *MetOp-A*, and *MetOp-B* (obtained from the COSMIC data center at http://www.cosmic.ucar.edu/). The first part of the record (2001–06) is based primarily on measurements from CHAMP (Wickert et al. 2001), while after 2006 a much larger dataset is available (including the six-satellite constellation from COSMIC; Anthes et al. 2008). The total number of occultations over the globe exceeds 6 200 000.

The GPS data record is illustrated in Fig. 1, showing the number of individual measurements in the near-equatorial band (10°N–10°S) for 5-day (pentad) samples covering 19 May 2001 to 29 September 2013 (902 pentads). Our analyses are based on pentad averages in

order to ensure adequate coverage and avoid missing data during the early part of the record (2001–06). Figure 1 shows that for the 10°N–10°S band there are approximately 80–100 observations per pentad during 2001–06 and ~600 to over 1000 per pentad afterward. While much of our focus is on the 10°N–10°S latitude band, we also include results based on zonal mean temperatures over the globe, derived from GPS data binned into 10° latitude bands; in that case, each bin has approximately half the number of observations per pentad as shown in Fig. 1 (or more, as GPS sampling is somewhat higher outside of the deep tropics). We analyze the data on a 0.2-km vertical grid.

Part of our focus includes variability of the cold point tropopause, defined simply as the coldest point in the profile of the zonal average pentad data (the cold point typically lies ~0.5 km above the thermal tropopause in the tropics). The altitude of the cold point varies seasonally between ~(16.5–17.5) km (e.g., Seidel et al. 2001). We calculate anomalies of cold point temperature by subtracting the mean annual cycle in a similar manner to temperature time series at specific altitude levels.

b. *Circulation statistics from ERA-Interim reanalysis data*

We also include analysis of circulation statistics derived from ERA-Interim reanalysis data (Dee et al. 2011) to complement the GPS temperatures. These include zonal mean winds, eddy heat, momentum and Eliassen–Palm (E–P) fluxes, and mean tropical upwelling derived from momentum balance ($\overline{w}_m^*$) (Randel et al. 2002; Abalos et al. 2012). We construct pentad averages of these data to directly match the time series of pentad GPS data.

c. *Spectrum analysis*

We include spectrum and cross-spectrum analysis of various time series to quantify frequency-dependent behavior. Spectra are calculated by direct Fourier transform of the 902-pentad time series, resolving periods of 4510 to 10 days [with a frequency resolution $\Delta\omega = (2\pi/4510 \text{ days})$]. Calculations are based on standard formulas in Jenkins and Watts (1968). Power spectra are smoothed using a Gaussian-shaped smoothing with half-width of $5\Delta\omega$. Coherence squared (coh^2) and phase spectra are calculated using a wider bandwidth ($20\Delta\omega$) to enhance statistical stability. This results in approximately 20 independent Fourier harmonics for each spectral estimate, and the resulting 95 and 99% significance levels for the coh^2 statistic are 0.15 and 0.22, respectively. The high- and low-frequency ends of the spectra are smoothed using one-sided Gaussian smoothing so that significance levels are somewhat higher.

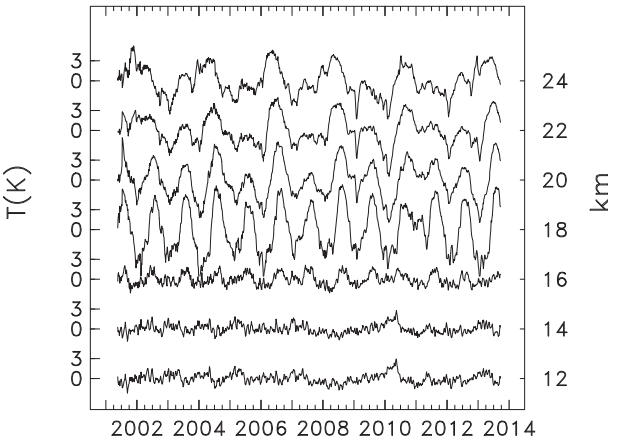

FIG. 2. Time series of zonal mean temperatures over 10°N–10°S at altitude levels 12, 14, . . . , 24 km. The time mean has been removed at each altitude and levels offset for clarity. The year labels refer to 1 Jan for each year.

3. Observations from GPS

a. *Tropical seasonal cycle, QBO, and ENSO*

Time series of pentad zonal mean temperatures over 10°N–10°S for altitudes 12, 14, 16, . . . , 24 km are shown in Fig. 2. A clear annual cycle is evident for altitudes ~(16–22) km (largest near 18 km), while there are small seasonal variations in the upper troposphere (at and below 14 km). We isolate and remove the seasonal variations at each altitude by harmonic analysis, including the first four annual harmonics. Time series of the deseasonalized temperature data (Fig. 3) show larger variability in the stratosphere (18 km and above) compared to the troposphere, which is primarily attributable to the QBO. The dominance of the QBO in the equatorial stratosphere is highlighted in Fig. 4, showing the deseasonalized GPS temperature anomalies over 10–35 km during 2001–13. The QBO is evident as downward propagating anomalies of up to ±4 K, reaching close to the altitude of the cold point tropopause (seasonally varying over 16.5–17.5 km).

In addition to the QBO, ENSO also exhibits a significant influence on zonal mean temperatures in the tropical upper troposphere–lower stratosphere (UTLS) (Randel et al. 2009). To study variability distinct from the forced QBO and ENSO signals, we isolate and remove these variations using a standard multivariate regression analysis:

$$T(t) = \text{A1} \times \text{QBO1}(t) + \text{A2} \times \text{QBO2}(t) + B \times \text{ENSO}(t). \quad (3)$$

Here QBO1(t) and QBO2(t) are orthogonal time series representing QBO variations, constructed from the equatorial zonal winds over 70–10 hPa (Wallace et al.

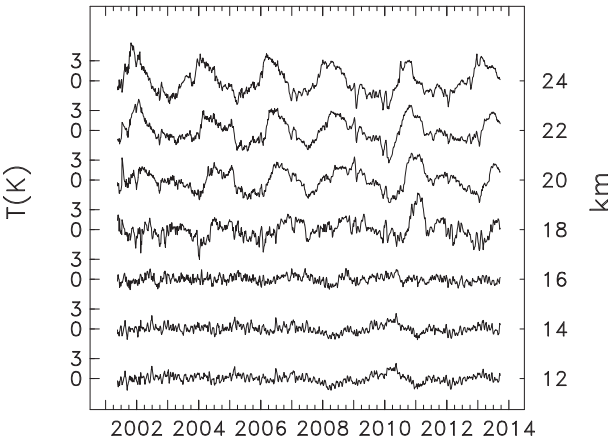

FIG. 3. Time series of deseasonalized zonal mean temperature anomalies over 10°N–10°S at altitude levels 12, 14, . . . , 24 km.

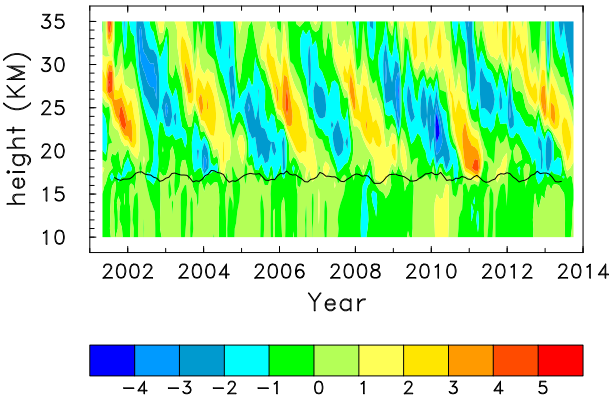

FIG. 4. Height–time section of deseasonalized zonal mean temperature anomalies (K) over 10°N–10°S. The black line denotes the altitude of the cold point tropopause.

1993), normalized to unit variance. ENSO(t) is the multivariate ENSO index (MEI) time series from the NOAA Climate Diagnostics Center (http://www.cdc.noaa.gov/people/klaus.wolter/MEI/). The strongest correlations with zonal mean temperature occur for a ~2-month time lag for the ENSO index (e.g., Calvo Fernández et al. 2004), which we use here. While the QBO1, QBO2, and MEI time series are available as monthly values, we interpolate to pentad values for application to the pentad GPS temperature data. The spatial structure of the terms A1 and B resulting from the regression fits to global GPS data are shown in Fig. 5. The QBO1 fit (Fig. 5a) shows equatorially centered QBO variations throughout the stratosphere with out-of-phase variations in the subtropics and middle latitudes (which are well known; e.g., Baldwin et al. 2001). There is a similar result for the QBO2 component (not shown here), which is spatially orthogonal with the patterns in Fig. 5a. The ENSO fit for temperature (Fig. 5b) shows warming in the tropical upper troposphere and cooling in the lower stratosphere focused in the deep tropics [~(20°N–20°S)]; note there is relatively little ENSO influence near the cold point tropopause, as this is near the node in vertical structure. The zonal mean warming of the troposphere is a well-known feature of ENSO (e.g., Yulaeva and Wallace 1994; Calvo Fernández et al. 2004; Scherllin-Pirscher et al. 2012), and the lower-stratospheric cooling (echoed in closely correlated zonal mean ozone variations) is a signature of enhanced upwelling in this region during positive ENSO events (Randel et al. 2009; Calvo et al. 2010; Simpson et al. 2011). For reference, Figs. 5c,d show the corresponding zonal wind variations for QBO1 and ENSO derived from regression of the ERA-Interim data. The QBO zonal winds are focused in the stratosphere over the equator, while ENSO modulates winds in the subtropics [~(10°–30°N and 10°–30°S)], extending from the upper troposphere well into the lower stratosphere (up to ~20 km).

b. *Residual temperature variability*

Removal of the QBO and ENSO variations from the deseasonalized tropical temperature anomalies results in the time series shown in Fig. 6. These "residual" time series represent the inherent variability of tropical zonal mean temperatures (linearly independent of the seasonal cycle, QBO, and ENSO fluctuations) and are the focus of the remainder of this work. As a note, inspection of the upper-tropospheric residuals in Fig. 6 (at 12 and 14 km) suggest some remaining ENSO variability that is not is removed by the linear regression onto MEI; that is, the residuals retain some ENSO-like behavior. The variance of the residual temperature time series is shown as a function of altitude in Fig. 7 and compared with the variance associated with QBO, ENSO, and seasonal components. The residual variance exhibits a relatively sharp maximum slightly above the cold point tropopause, with a similar vertical structure as the seasonal cycle (which is by far the largest component of variance in the deep tropics). The residual dominates the deseasonalized variability near the tropopause; that is, it is much larger than QBO or ENSO influences. This isolated temperature variance maximum near the tropopause is consistent with previous observations from radiosondes (Sato et al. 1994) or GPS data (Randel et al. 2003), although most previous studies have focused on statistics from individual measurements that reflect local wave variability. In contrast, Fig. 7 shows that the enhanced variance near and above the tropopause is a fundamental characteristic of the zonally averaged temperature.

We further explore the residual variability based on empirical orthogonal function (EOF) analysis of the residual time series (e.g., Fig. 6) over 10–30 km. This results in two dominant modes (termed EOF1 and EOF2),

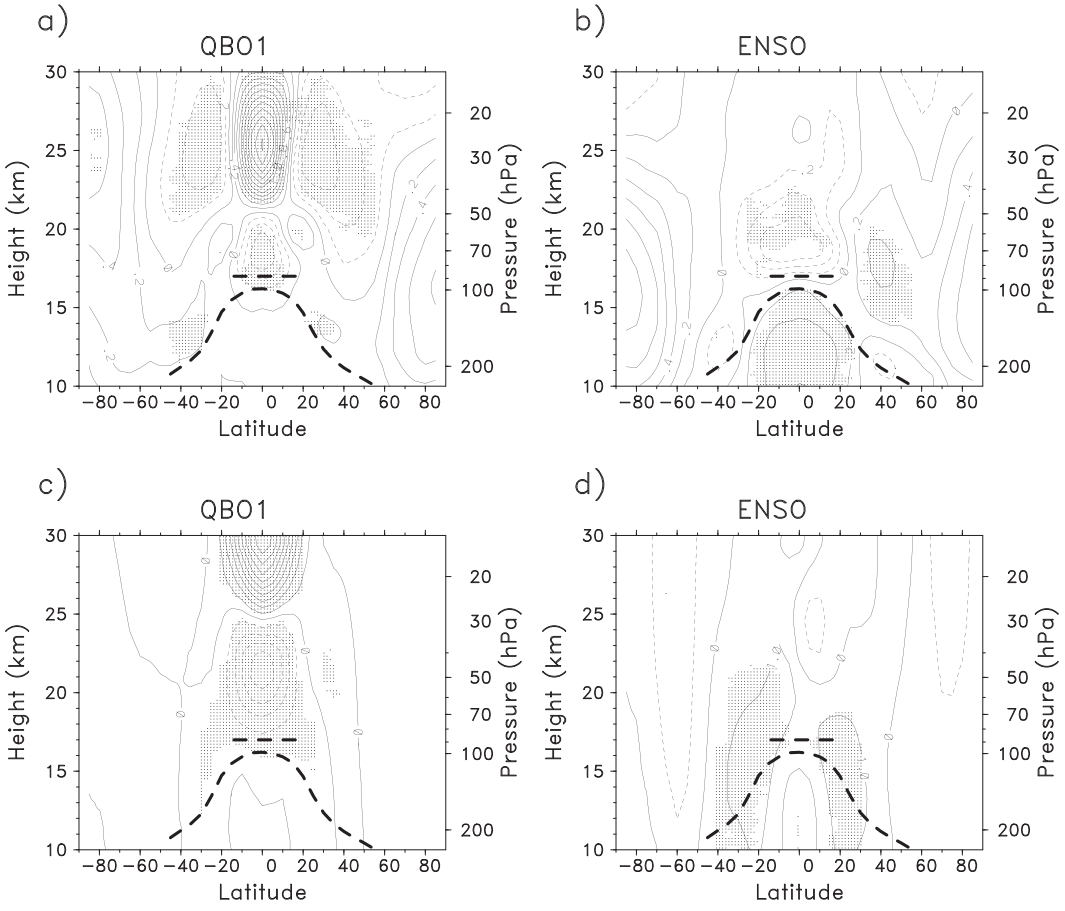

FIG. 5. Meridional cross sections of the regression-derived zonal mean temperature variation linked with (a) QBO1 and (b) ENSO in Eq. (2). Contours (with interval 0.2 K and negative dashed) show temperature variations linked to one-sigma standard deviations of the respective proxy time series, and shading shows where the fits are statistically significant at the 3 × sigma (99%) level. There is a corresponding QBO2 pattern (not shown) that has similar magnitude and is spatially orthogonal to QBO1. Corresponding patterns in zonal mean zonal winds, derived from ERA-Interim data, with contour intervals of (c) 2 and (d) 1 m s^{-1}. The heavy dashed lines denote the thermal and cold point tropopauses.

explaining 73% and 18% of the overall variance, respectively. These modes are statistically significant and well separated from higher EOFs (EOF3 has 4% variance). The exact vertical structures of EOF1 and EOF2 are somewhat dependent on the vertical domain of the calculations, but the characteristic behavior separating variability above ~20 km from the near-tropopause region (discussed below) is a robust result. As a note, we have not weighted these altitude-dependent EOF calculations with the square root of density, as this would deemphasize the stratospheric variability.

The vertical structure and corresponding expansion coefficient [or principal component (PC)] time series of the two modes are shown in Fig. 8. EOF1 exhibits a vertical structure with broad maximum values in the stratosphere (at and above 18 km) and small values below, and we term this the "deep stratosphere mode." The PC1 time series (Fig. 8b) is characterized by large month-to-month variability, discussed further below. The EOF2 spatial structure shows a relatively narrow maximum peaking near 18 km, similar to the residual variance maximum in Fig. 7, and we term this the "near-tropopause mode." The PC2 time series (Fig. 8b) are similar to the residual anomalies at 18 km seen in Fig. 6.

Time series of temperature anomalies associated with the deep stratosphere mode (PC1) reveal clues to forcing of this variability. Two especially large negative (cooling) events are evident in Fig. 8b (each larger than 4 × sigma variability) in September 2002 and January 2009 (labeled A and B in Fig. 8b). These correspond to well-known large stratospheric sudden warming events [September 2002 in the Southern Hemisphere (Newman and Nash 2005) and January 2009 in the Northern Hemisphere (Manney et al. 2009)]. Meridional cross

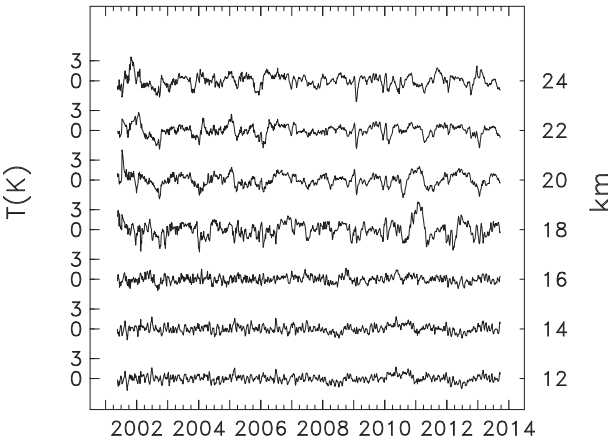

FIG. 6. Time series of residual zonal mean temperature anomalies over 10°N–10°S. Residuals are calculated by removing the seasonal cycle, QBO, and ENSO components via regression.

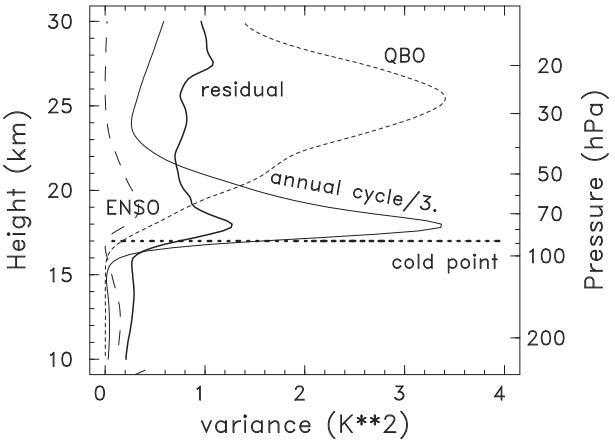

FIG. 7. Vertical profile of temperature variance in the deep tropics (10°N–10°S) associated with annual cycle, QBO, ENSO, and residual variability. The variance for the annual cycle has been divided by three to fit within this scale. The horizontal dashed line denotes the altitude of the time average cold point tropopause.

sections of global temperature anomalies derived from GPS data for the respective pentads are shown in Figs. 9a,b. The anomalies in Figs. 9a,b show approximate mirror-image patterns: large warming in the winter polar regions and cooling in the tropics as a response to global-scale overturning circulations (e.g., Dunkerton et al. 1981; Garcia 1987). The tropical cooling in Figs. 9a,b shows interesting symmetry, with cold anomalies centered over the equator above ~22 km, but low-latitude anomalies shifted toward the winter hemisphere below this level. The temperature anomalies show relatively small influence near the tropical tropopause in both cases.

In general, we find that many of the individual cooling spikes for PC1 in Fig. 8b are related to high-latitude warming events, and tropical temperature anomalies associated with the deep stratosphere mode are linked to global-scale latitudinal see-saw variations focused in the winter hemisphere. This behavior is illustrated by regressing the PC1 time series onto the global pentad temperature anomalies and making separate calculations during NH winter (December–March) and SH winter (June–September). These temperature patterns (Fig. 10) show high-latitude warming in the winter hemisphere and tropical cooling, with somewhat stronger effects during NH winter. Regressions onto zonal winds show corresponding weakening of the polar night jets in each winter hemisphere (results not shown).

There are also high correlations between the PC1 time series and variations in planetary wave forcing in winter high latitudes, as quantified by regressions onto the Eliassen–Palm (E–P) flux, also shown in Fig. 10. In these calculations, the E–P fluxes are lagged by two pentads (E–P fluxes preceding PC1) to maximize the signal, which is consistent with wave fluxes preceding strongest stratospheric temperature effects. The results in Fig. 10 show enhanced upward E–P fluxes in the respective winter hemisphere preceding the changes in stratospheric temperature and circulation. These results are consistent with the well-known seasonal cycle of stratospheric planetary waves in each hemisphere. This overall behavior is consistent with transient extratropical wave forcing of the equatorial stratosphere, as highlighted in previous studies (Randel 1993; Ueyama and Wallace 2010; Ueyama et al. 2013; Grise and Thompson 2013; Gómez-Escolar et al. 2014).

The tropical tropopause mode (EOF2) shows distinct spatial and temporal structure. Figure 11a shows a regression map of global temperature residuals onto the time series of PC2, highlighting a strong maximum in the tropical lower stratosphere, centered slightly above but overlapping the time mean cold point. The patterns in Fig. 11a also show weaker negative regressions in the tropical upper troposphere (which are statistically significant), and this coupling with the tropical troposphere is important for understanding forcing of near-tropopause variability. Figure 11b shows a complementary calculation of a one-point correlation map for temperature residuals with respect to a reference position at the equator and 12 km, highlighting a similar out-of-phase behavior between the tropical upper troposphere and lower stratosphere. The patterns in Fig. 11b are similar to the ENSO spatial structure in Fig. 5b and also to the zonal mean temperature response to Madden–Julian oscillation (MJO) variations in the tropical troposphere (Virts and Wallace 2014). In both cases (ENSO and MJO), the lower-stratosphere temperature anomalies are a response to variations in upwelling in the tropical lower stratosphere (Calvo et al. 2010; Virts and Wallace 2014).

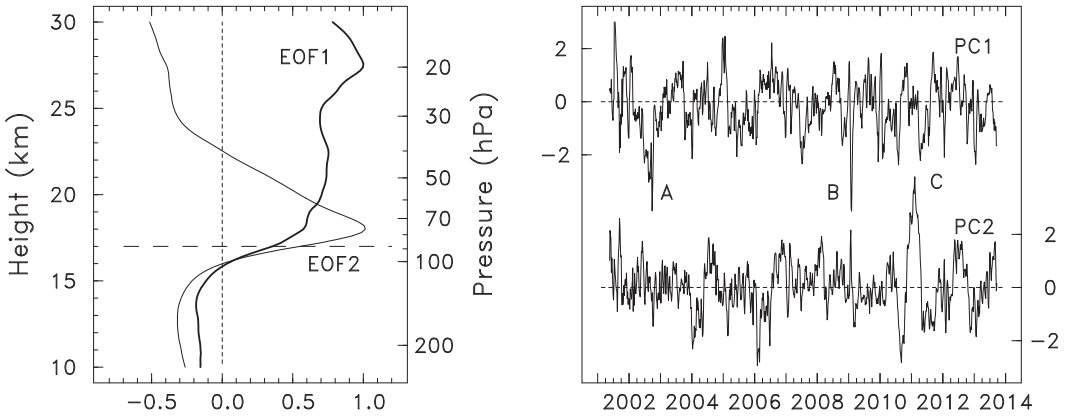

FIG. 8. Results of an EOF analysis of zonal mean temperature residuals over 10°N–10°S, showing (a) the vertical structures for EOF1 and EOF2 and (b) the respective principal components PC1 and PC2. The vertical structures are normalized to a maximum value of 1.0, and the respective time series are normalized to unit variance. The labels A, B, and C refer to extreme events shown in Figs. 9 and 17.

Relationships between the tropical upper troposphere and lower stratosphere are quantified further in Fig. 12, showing time series of tropical (10°N–10°S) temperature residuals at 12 and 18 km, and also at the cold point tropopause. Figure 12 includes time series for the full deseasonalized temperature anomalies (Fig. 12a) and also for residuals with QBO and ENSO effects removed via regression (Fig. 12b); comparisons show the relatively small but nonnegligible influence of QBO near the tropopause. Variability in the cold point temperature is highly correlated with 18 km ($r = 0.74$), but this correlation peaks sharply in altitude (Fig. 13), so that the cold point is poorly correlated with altitudes above 20 km and below 16 km. Time series in Fig. 12 highlight the enhanced variability of temperatures near the tropopause and in the lower stratosphere compared to the upper troposphere and frequent out-of-phase behavior. Temporal power spectra of the time series at 12 and 18 km are shown in Fig. 14a, and while enhanced variability at 18 km occurs across the entire spectrum, the enhancement is larger for low frequencies (seasonal to interannual time scales); we show below that this behavior is attributable to the long radiative relaxation time scales in the lower stratosphere. Calculation of the coherence squared between the time series at 12 and 18 km (Fig. 14b) shows that the strongest coherence occurs for a broad band with oscillation periods centered near 30–60 days, which is likely a signature of a physical mechanism linked to the MJO (Virts and Wallace 2014). Figure 14a also indicates that temperature variations are out of phase between 12 and 18 km across the entire spectrum.

The spatial structure of zonal mean temperatures for the MJO based on GPS data are shown in Fig. 15a, derived from regression onto temperatures at the equator

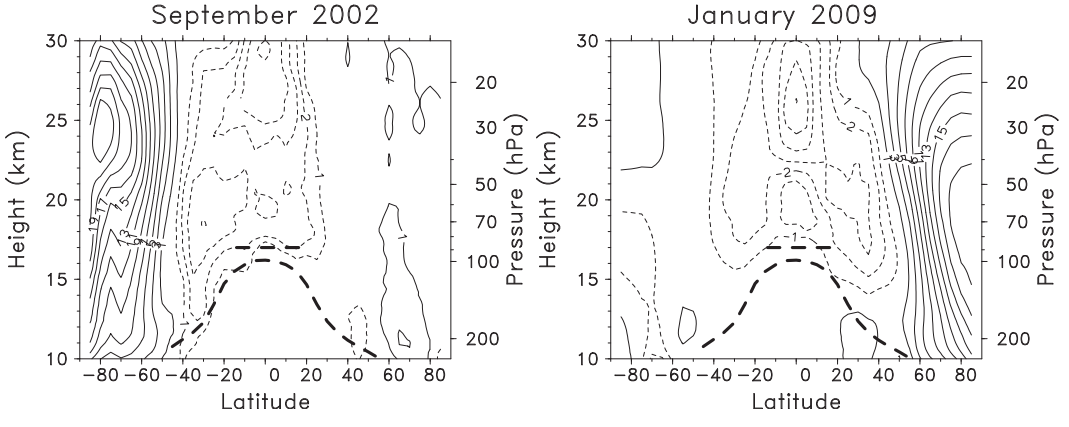

FIG. 9. Meridional cross sections of pentad temperature anomalies associated with strong negative projections of PC1 during September 2002 and January 2009 (noted A and B in Fig. 8b). These events are tied to strong stratospheric polar warming events. Contour interval is 1 K for negative contours and 2 K for positive contours, with zero contours omitted.

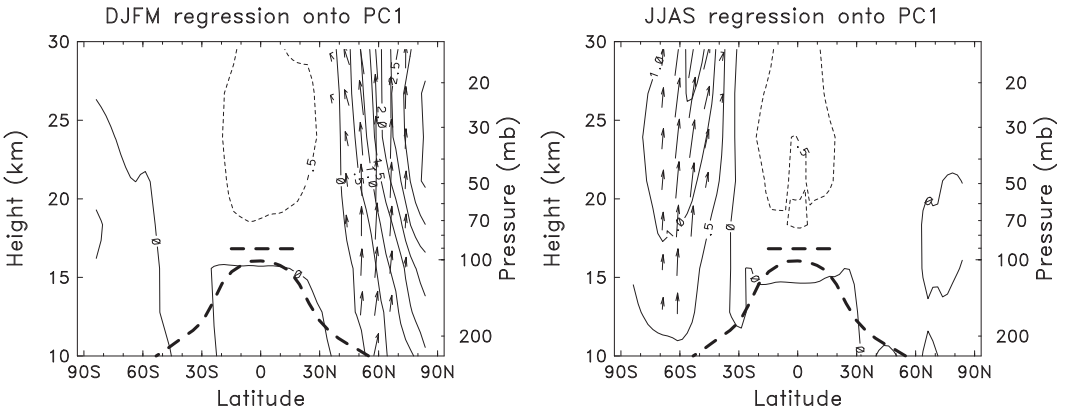

FIG. 10. Contours show regressions of zonal mean GPS temperatures (K) onto normalized PC1 time series for calculations during (left) NH winter (December–March) and (right) SH winter (June–September). Vectors show the corresponding regressions onto the E–P fluxes during these seasons. The E–P fluxes are lagged by two pentads to maximize the regressions (E–P fluxes preceding PC1), and arrows are only shown at locations where the respective correlations are statistically significant.

and 12 km that have been bandpass filtered for periods 25–80 days. Figure 15a shows temperature anomalies of ~0.3 K in the tropical upper troposphere with similarly sized out-of-phase variations over ~(16–19) km (centered near or slightly above the cold point tropopause). Figure 15b shows the corresponding zonal mean wind MJO variations derived in a similar manner from ERA-Interim data, highlighting wind anomalies centered near the equator mainly confined to the troposphere. Note that the temperatures and winds in Figs. 15a,b are in thermal wind balance and that the negative temperature anomalies near the tropopause are in balance with the strong wind shears in this region.

The frequency-dependent behavior of vertical coherence the GPS temperatures with respect to the upper troposphere is quantified in Fig. 16a, which shows the coh^2 as a function of altitude and frequency with respect to a reference altitude of 12 km. Temperature variability in the upper troposphere is coherent over altitudes up to ~(15–16) km over all time scales, while the vertical structure of coherence with the lower stratosphere changes as a function of frequency. For low frequencies (periods greater than ~180 days) significant coh^2 (out of phase with the upper troposphere; not shown) is found over a relatively narrow altitude range of ~(19–20) km. This behavior is similar to that derived for the ENSO regression (Fig. 5b), and in fact the low-frequency statistical signature in Fig. 16a may reflect ENSO-like variations not removed in the linear regressions. The strongest lower-stratosphere coh^2 in Fig. 16a occurs for a broad band of periods centered near 30–60 days (as in Fig. 14b), and here the maximum coh^2 occurs at lower altitudes of ~(16–20) km. We

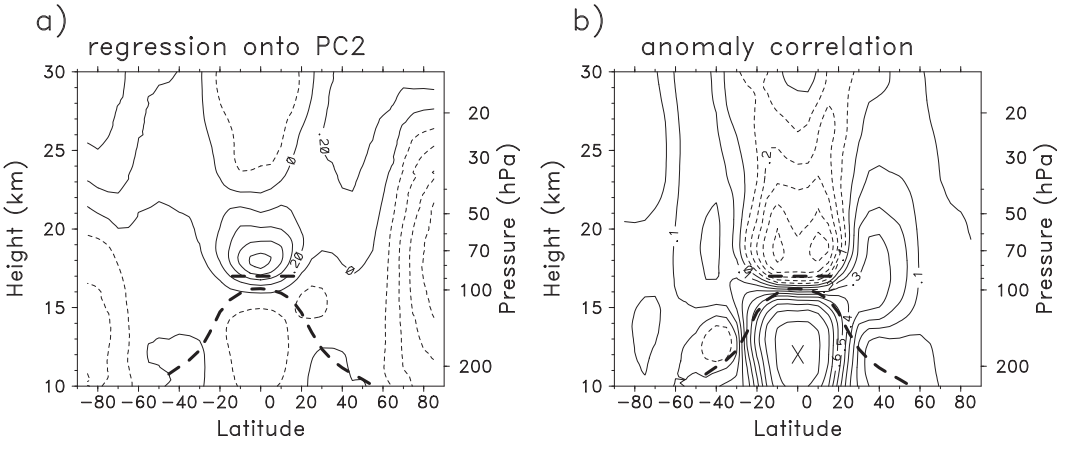

FIG. 11. (a) Meridional cross section of residual temperature anomalies (K) regressed onto normalized PC2 time series. (b) One-point correlation map for zonal mean temperature residuals with respect to variations in the tropical upper troposphere (12 km).

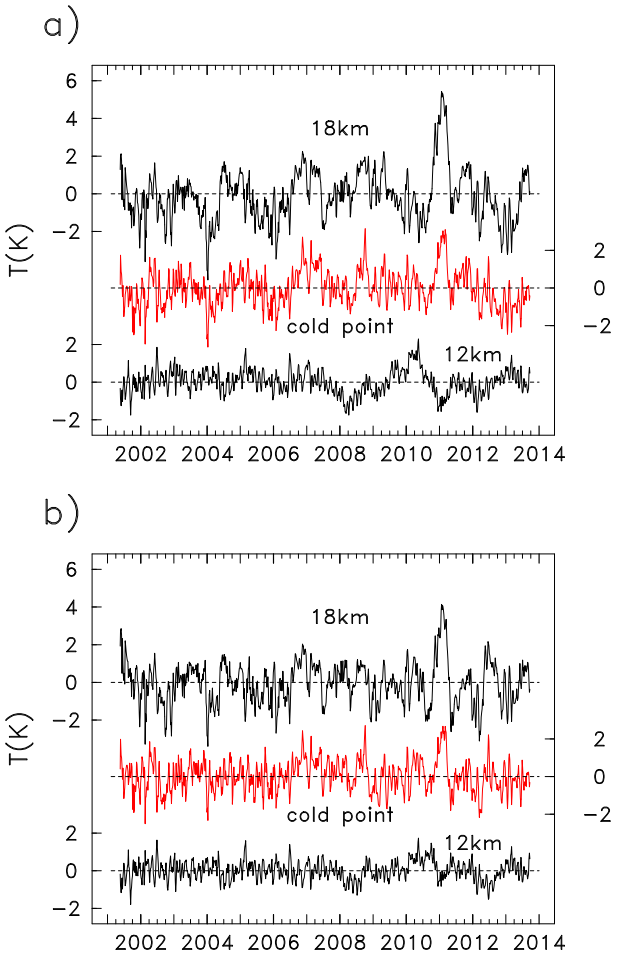

FIG. 12. (a) Time series of deseasonalized zonal mean temperature anomalies over 10°N–10°S at 12 and 18 km and at the cold point. (b) As in (a), but additionally the QBO and ENSO components have been removed via regression (i.e., temperature residuals).

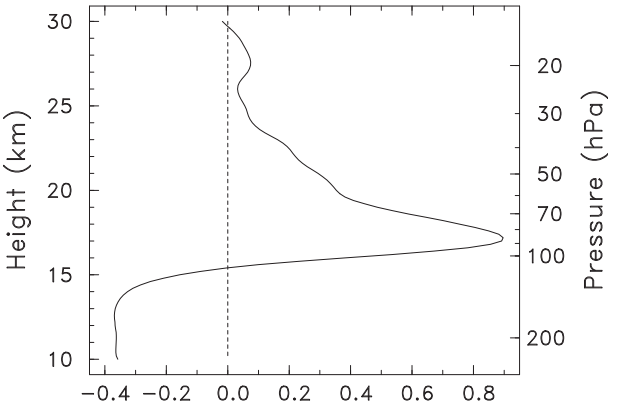

FIG. 13. Vertical profile of the correlation of zonal mean temperature residuals with respect to the cold point tropopause.

note that there is highly significant coh^2 near the altitude of the cold point (~17 km) for ~(30–60)-day periods in Fig. 16a (similar to the behavior in Fig. 15a), but not for shorter or longer time scales; for annual to interannual variations the cold point occurs near the node in vertical structure, as observed for ENSO (Fig. 5b).

A complementary calculation is shown in Fig. 16b, where coh^2 with respect to the cold point tropopause (i.e., the time series in Fig. 12b) is plotted as a function of frequency and altitude. Figure 16b shows that the cold point is highly coherent with altitudes ~(16–20) km over all frequencies (weekly to interannual time scales), while significant coherence with the upper troposphere occurs only for the band centered near ~(30–60) days. Hence, the out-of-phase behavior between the cold point tropopause and tropical upper troposphere seen in Fig. 13 is focused on MJO time scales, and there is no significant coherence between these regions at periods longer than ~100 days. This has important implications regarding control of the cold point on seasonal or interannual time scales, as discussed further below.

A remarkable event occurs in the PC2 time series and near-tropopause temperatures during 2010/11 (labeled as C in Fig. 8b), with persistent warm anomalies above 4 K at 18 km and over 2 K at the cold point (see Fig. 12b). This exceptionally warm anomaly in cold point temperature is clearly reflected in stratospheric water vapor observations (Randel and Jensen 2013). The spatial patterns of temperature anomalies for this period are shown in Fig. 17, showing localized warming in the tropical lower stratosphere together with cold anomalies in the tropical troposphere, tropical middle stratosphere, and Arctic stratosphere (these patterns are very similar to the global regressions onto PC2 in Fig. 11a, which may in fact be influenced by this extreme event). These signatures suggest that the anomalous near-tropopause warming may be related to the combined effects of 1) stratospheric response to a strong La Niña tropospheric event during 2010/11, 2) downward propagating warm QBO temperatures, and 3) reduced global Brewer–Dobson circulation (reflected in the persistent and anomalously cold Arctic stratosphere during this year; e.g., Manney et al. 2011). Although the effects of the QBO and ENSO have been removed via linear regression to derive residuals, the occurrence of large residuals coincident with the timing of QBO and ENSO variations (as seen in Fig. 4) suggest interactions that are not modeled by the linear QBO and ENSO regressions (in addition to possible coupling with the global BDC). This event is poorly understood at present.

c. *Understanding enhanced temperature variance in the tropical lower stratosphere*

Variability of zonal mean temperature in the tropical lower stratosphere is primarily forced by mean tropical

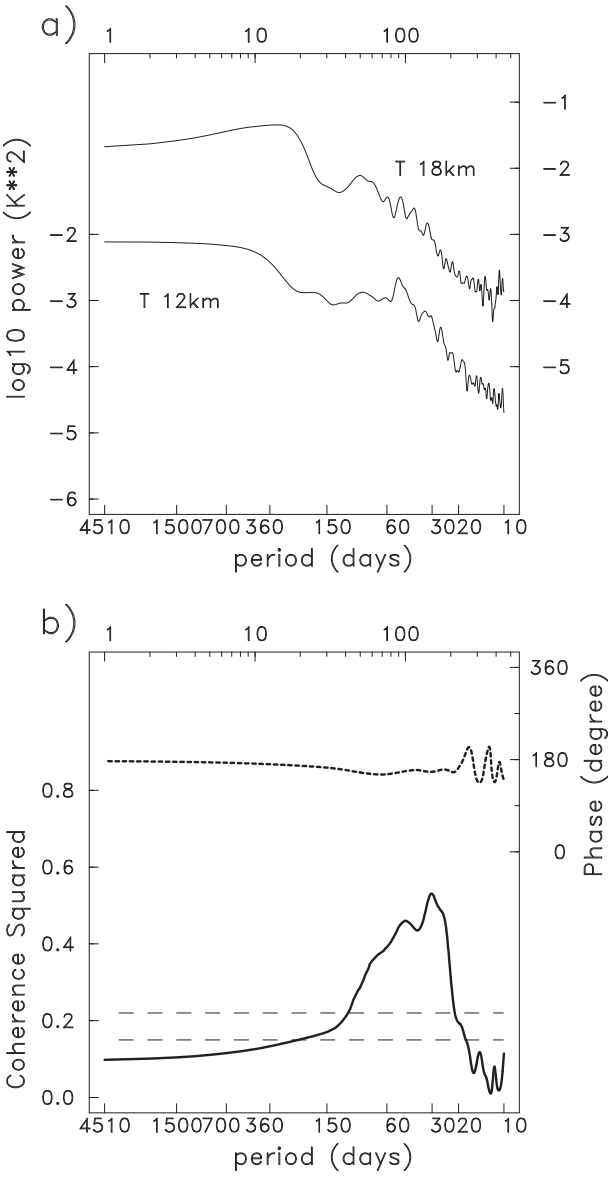

FIG. 14. (a) Temporal power spectra for zonal mean temperature residuals at 12 and 18 km plotted on log power vs log frequency axes. The top axis indexes the frequency spectral estimate, while the bottom axis shows the corresponding period in days. (b) Coherence squared and phase spectra between temperatures at 12 and 18 km. The dashed lines denote 95% and 99% significance levels.

upwelling (e.g., Abalos et al. 2012, 2013). The relationship between temperature and upwelling can be quantified by the simplified TEM thermodynamic equation, incorporating a linear relaxation approximation to radiative damping [Eq. (2)]:

$$\overline{T}_t = -\overline{w}^* S - \alpha(\overline{T} - \overline{T}_{\rm eq}). \tag{4}$$

Assuming harmonic variations of the form $[\overline{T}, \overline{w}^*] = \sum [T_\sigma, w_\sigma] \exp(i\sigma t)$, Eq. (4) reduces to a simple expression (Randel et al. 2002):

$$\sqrt{T_\sigma^2/w_\sigma^2} = S/\sqrt{\alpha^2 + \sigma^2}. \tag{5}$$

This expresses the temperature sensitivity to upwelling as a simple function of frequency and the radiative damping time-scale α^{-1}. It is well known that radiative damping time scales are long (α small) in the lower stratosphere, and a simple hypothesis is that the enhanced zonal mean temperature variance near the tropical tropopause (Fig. 7) is directly linked to the long radiative time scales in this region.

We test this hypothesis using GPS temperature time series in combination with estimates of $\overline{w}^*$ derived from ERA-Interim data. This is similar to the analysis in Randel et al. (2002), but extended to interannual time scales, which more effectively constrain the low-frequency behavior (see discussion below). We calculate $\overline{w}^*$ estimated from the zonal mean momentum balance (referred to as $\overline{w}^*_m$) from ERA-Interim data during 2001–13, evaluated for the latitude band 20°N–20°S and standard ERA-Interim pressure levels (as in Abalos et al. 2012). Daily time series of $\overline{w}^*_m$ are averaged into pentads, and these time series (e.g., shown for 80 hPa in Fig. 18) exhibit an annual cycle in addition to large variability at subseasonal time scales (Abalos et al. 2014). We remove the seasonal cycle, QBO, and ENSO variations to generate residual $\overline{w}^*_m$ anomalies (the seasonal cycle is relatively large, while the QBO and ENSO fits are relatively small for $\overline{w}^*_m$ at 80 hPa).

Power spectra for $\overline{w}^*_m$ (80 hPa) and GPS temperature residuals at 18 km are shown in Fig. 19a. The power spectrum for $\overline{w}^*_m$ is much flatter in frequency than the red temperature power spectrum at frequencies higher than the annual cycle, while at low frequencies they are equally flat. This is precisely what Eq. (5) predicts: $(T_\sigma/w_\sigma) \sim \alpha^{-1}$ (independent of σ) when $\alpha \gg \sigma$, and $(T_\sigma/w_\sigma) \sim \sigma^{-1}$ when $\sigma \gg \alpha$. Note that for $\alpha \sim (30\,\text{days})^{-1}$, $\sigma \sim \alpha$ for frequencies near $(2\pi/180\,\text{days})^{-1}$ (indicated with the vertical dashed lines in Fig. 19), so that both frequency extremes are spanned in these data. Coherence squared spectra between $\overline{w}^*_m$ and T (not shown) reveal significant coherence over most of the frequency range. More importantly, the relative magnitude of temperature and vertical velocity variations [$R_\sigma = \sqrt{T_\sigma^2/w_\sigma^2}$, as in Eq. (5)] can be quantified by these data, giving an estimate of temperature response to vertical velocity at each frequency. Figure 19b shows that R_σ varies in frequency by approximately a factor of 10, increasing substantially for periods longer than

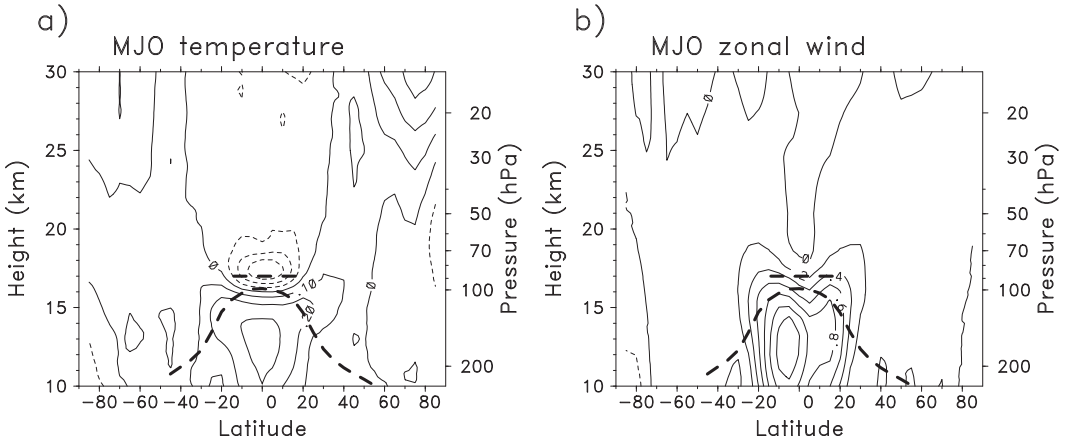

FIG. 15. Meridional cross sections of (a) GPS temperatures (K) and (b) ERA-Interim zonal winds ($m\,s^{-1}$) associated with the MJO. These results are calculated as regressions onto the GPS temperatures at the equator and 12 km, filtered to isolate variations with 25–80-day periods.

100–200 days (including the seasonal cycle and longer periods). In other words, temperature exhibits a much stronger response to $\overline{w}^*$ at low frequencies, and this is the cause of the enhanced low-frequency temperature variance in Fig. 19a (and larger low-frequency temperature variance at 18 km compared to 12 km in Fig. 14).

The estimates of R_σ derived from data can be compared to results predicted from the simple thermodynamic balance in Eq. (5) (i.e., $S/\sqrt{\alpha^2+\sigma^2}$) for various values of the radiative time-scale α^{-1} (with S derived from the background temperature structure). Figure 19b includes this comparison, showing that the ratio derived from the $\overline{w}^*_m$ and T observations agree remarkably well with the frequency dependence of the theoretical ratio, using α^{-1} of 25–30 days. In fact, the availability of a decade-long record of T and $\overline{w}^*$ observations provides novel characterization of the damping time-scale α^{-1}, as R_σ is only sensitive to α at periods greater than 1 yr (Fig. 19b). Similar calculations at other standard pressure levels (Fig. 20) show a strong enhancement of α^{-1} in the lower stratosphere, echoing the vertical structure of the residual variance (and the seasonal cycle) in Fig. 7. We note that these calculations apply explicitly to zonal mean variations, while in general the local radiative damping time scale in the tropical lower stratosphere is strongly dependent on the vertical scale of wavelike variations (e.g., Hartmann et al. 2001; Hitchcock et al. 2010). We conclude that the observed zonal mean temperature variance

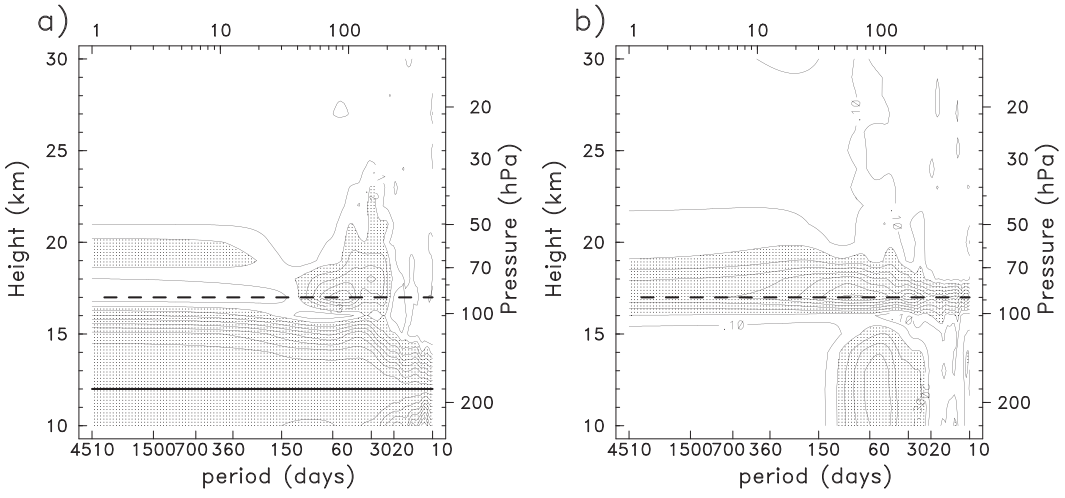

FIG. 16. (a) Altitude–frequency section of coherence squared for zonal mean temperature residuals with respect to a reference altitude of 12 km (dark solid line). Contour interval is 0.1, and shaded values (above 0.2) are significant near the 99% level. (b) As in (a), but using a reference time series of the cold point tropopause (shown in Fig. 12b). The dark dashed lines in (a),(b) indicate the mean altitude of the cold point tropopause.

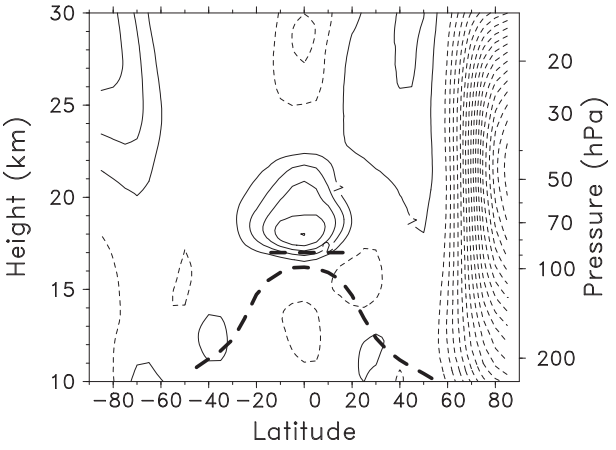

FIG. 17. Meridional cross section of temperature anomalies for the 25 days spanning 10 Feb–6 Mar 2011 (noted as C in Fig. 8b). Contour interval is 1 K, with zero contours omitted.

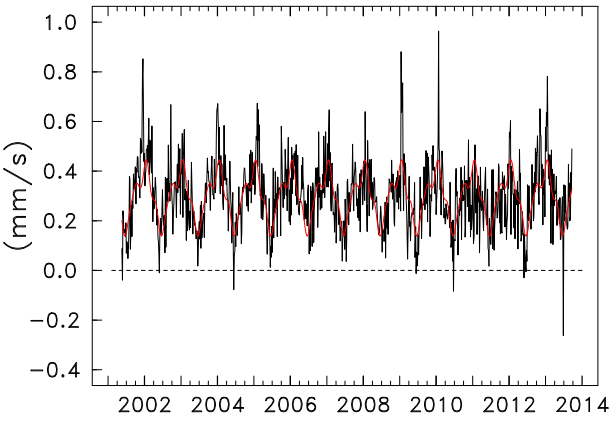

FIG. 18. Time series of pentad average vertical velocity at 20°N–20°S, 80 hPa derived from ERA-Interim data, calculated from momentum balance ($\overline{w}^*_m$; Abalos et al. 2012). The red line shows the average seasonal cycle.

maximum in the lower stratosphere is consistent with independently derived w^* behavior and that the relative maximum in residual temperature variance (and large annual cycle) near 18 km (Fig. 7) is directly related to the relatively long radiative time scales in this region.

4. Summary and discussion

GPS temperature measurements provide a unique high-vertical-resolution dataset to examine variability of tropical temperatures, with dense data coverage for more than a decade. Our focus on zonal mean temperature is motivated by interpretations via highly simplified theory, and we aim to improve understanding of variability and physical links between the upper troposphere, tropopause region, and stratosphere. The GPS data furthermore provide accurate resolution of the cold point tropopause, which exerts a controlling influence on stratospheric water vapor. Part of our objective is to understand variability of the cold point and its relation with tropospheric and stratospheric temperatures.

GPS data during 2001–13 reveal the well-known seasonal cycle, QBO, and ENSO influences on tropical temperatures, with distinct and physically robust spatial patterns (Fig. 5). However, our main focus is on quantifying residual temperature variability after removal of these large-scale forced variations; this residual signal may be equated to natural "climate" fluctuations (in addition to the QBO and ENSO signals) of the tropical atmosphere across a broad temporal spectrum. Residual variability over 10–30 km is primarily explained by two empirical modes: one focused in the deep stratosphere and one near the tropical tropopause. These distinct modes emerge naturally from EOF analysis of tropical temperatures, and this statistical signature is consistent with distinct upper and lower branches of the Brewer–Dobson (BD) circulation (e.g., Plumb 2002; Birner and Bönisch 2011). The upper branch is statistically linked to out-of-phase temperature changes in polar latitudes and shows strong correlations with high-latitude planetary wave fluxes (Fig. 10), which is consistent with well-known behavior (e.g., Ueyama and Wallace 2010; Abalos et al. 2014). Two exceptionally large tropical cooling events are seen in the GPS data record, associated with extreme stratospheric sudden warming events in the SH (September 2002) and NH (January 2009). The GPS temperature measurements reveal interesting mirror-image patterns for these events (Fig. 9), with equatorially symmetric cooling above ~22 km and low-latitude cooling shifted toward the winter hemisphere at lower altitudes. We do not know of a simple explanation for this behavior.

The near-tropopause mode is relatively narrow in altitude centered over [~(17–20) km] and exhibits weak out-of-phase behavior with temperatures in the upper troposphere. In a consistent manner, anomaly correlations with tropical upper-tropospheric temperatures (Fig. 11b) show out-of-phase temperature variations in the lower stratosphere, with patterns suggesting shallow circulation cells with reversed flows in midlatitudes [~(30°–60)°N/S]. This latter behavior is consistent with the lower-branch BD circulations identified in Birner and Bönish (2011) and Abalos et al. (2014). The cold point tropopause is closely related to the lower branch and weakly out of phase with temperatures in the upper troposphere.

Coherence between the tropical upper troposphere and lower stratosphere shows a maximum for variations for a broad band with periods near ~(30–60) days, which we interpret as a fingerprint of the MJO. The spatial pattern of zonal mean temperatures for this frequency band (Fig. 15a) show out-of-phase variations between

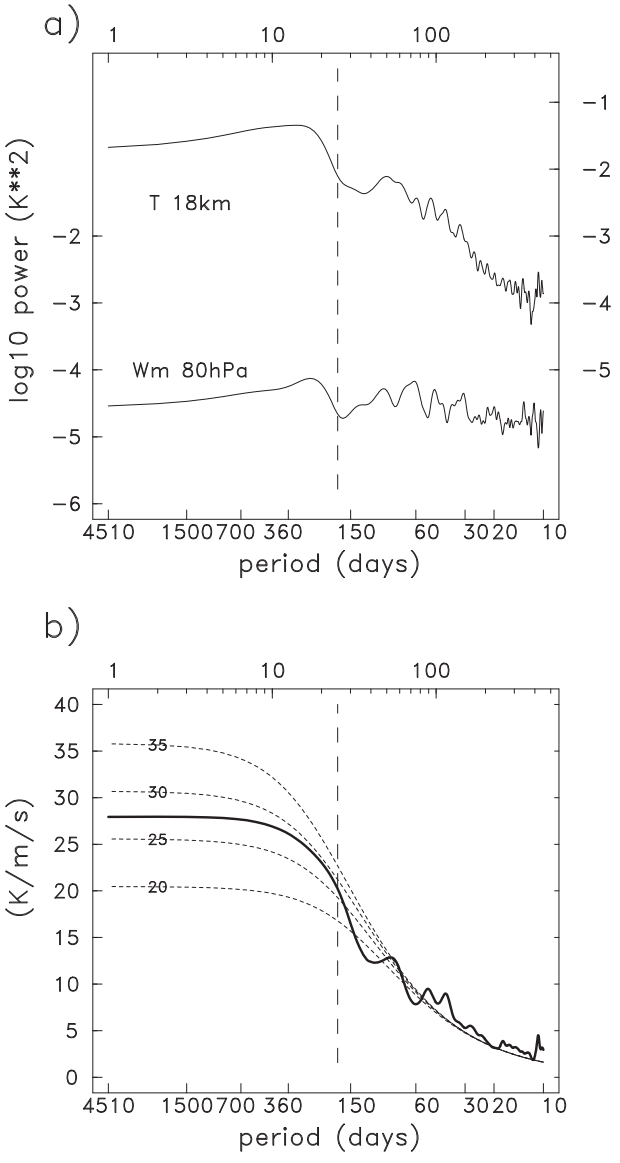

FIG. 19. (a) Power spectra of ERA-Interim $\overline{w}_m^*$ at 80 hPa and GPS zonal mean temperature at 18 km. (b) Ratio of temperature to upwelling ($R_\sigma = \sqrt{T_\sigma^2/w_\sigma^2}$) as a function of frequency. Results in (a),(b) are based on residuals, with seasonal cycle, QBO, and ENSO effects removed. The light dashed lines show corresponding theoretical behavior linked to the thermodynamic balance [$S/\sqrt{\alpha^2+\sigma^2}$, Eq. (5)], for radiative damping time scales of 20–35 days. The vertical dashed lines indicate the region where $\sigma \sim \alpha$ for $\alpha = (30\,\text{days})^{-1}$.

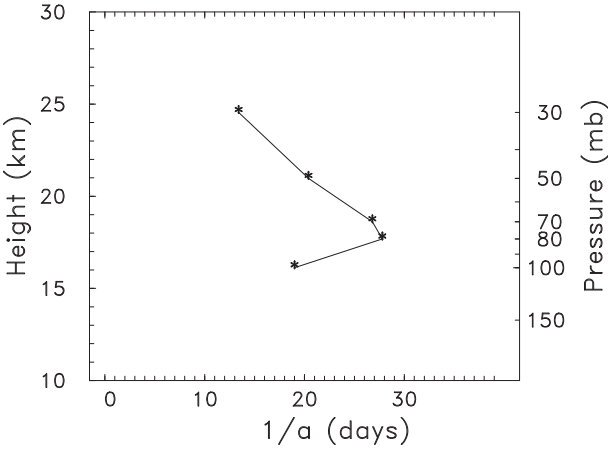

FIG. 20. Vertical profile of radiative damping time scales derived from fitting observed and theoretical zonal mean temperature/upwelling ratios from ERA-Interim $\overline{w}_m^*$ and GPS temperatures (as in Fig. 19).

the upper troposphere and lower stratosphere, with the latter focused near the cold point tropopause. The MJO influences on tropical circulation, clouds, and chemical composition has recently been described by Virts and Wallace (2014), and their results for zonal mean variations are consistent with the results here.

Zonal mean temperature variations at the cold point tropopause are most strongly correlated with temperatures over a relatively narrow altitude region ~(16–20) km (Fig. 13), primarily linked to dynamically forced upwelling (see below). Strongly coherent out-of-phase variations between the cold point and tropical upper-tropospheric temperatures are found for MJO time scales (Figs. 15a and 16), but there is little coherence with the upper troposphere for time scales longer than ~100 days (consistent with the very small ENSO impact on the zonal mean cold point seen in Fig. 5b). Virts and Wallace (2014) have shown that the MJO cold point temperature variations are reflected in zonal mean stratospheric water vapor and tropopause cirrus amounts. While strong coherence between the cold point and the upper troposphere occurs for MJO time scales, our results show that the cold point (and, by inference, stratospheric water vapor and tropopause cirrus) is not strongly tied to upper-troposphere temperatures at seasonal or interannual time scales. We note that the lack of coherence with the cold point at seasonal or interannual time scales implies there is no simple climate feedback between upper-tropospheric temperatures and stratospheric water vapor entering across the tropical tropopause, which is in contrast to the behavior inferred by Dessler et al. (2013).

The lower-stratosphere temperature response to the MJO is centered near the cold point tropopause [~(16–19) km], while the patterns for ENSO or other interannual time scales are somewhat higher [~(17–22) km], with a node near the cold point. What processes account for this difference? The lower-stratospheric temperatures in both cases (MJO and ENSO) are the response to dynamically forced upwelling, so that the altitude of the upwelling determines the vertical temperature response. While the tropical thermal structures for ENSO and MJO are broadly similar (Figs. 5b and 15a), they have very

distinctive signatures in the zonal wind field; the MJO is centered near the equator in the tropical upper troposphere (Fig. 15b), while ENSO variations maximize in the subtropics and extend well into the lower stratosphere (Fig. 5d). The eddy forcing associated with the zonal mean MJO occurs primarily from equatorial planetary waves in the upper troposphere, with resultant forced upwelling near the tropopause (e.g., Grise and Thompson 2012; note similar behavior in the idealized calculations of Norton 2006). In contrast, model calculations (Calvo et al. 2010; Simpson et al. 2011) suggest that the ENSO subtropical zonal wind anomalies influence wave dissipation in the lower stratosphere (from extratropical large-scale waves and gravity waves), modulating upwelling at levels above the tropopause. These differences in zonal winds and wave forcing details may contribute to the distinct vertical structures of the MJO and ENSO temperature responses in the lower stratosphere.

Temperatures near the tropical tropopause are highly correlated with upwelling in the lower stratosphere, driven by transient subtropical wave forcing in addition to high-latitude planetary waves (Abalos et al. 2014). The derived frequency dependence of this relationship (Fig. 19b) reveals that temperature response to upwelling is strongly enhanced (by an order of magnitude) for relatively low frequencies (periods longer than ~0.5 yr). This behavior is remarkably well explained by the idealized thermodynamic balance in Eq. (5), incorporating a linear thermal damping with a relaxation time scale of ~30 days. These calculations provide a sensitive empirical measure of radiative damping time scales appropriate for zonal mean tropical temperatures, highlighting a relatively narrow maximum for long radiative time scales in the tropical lower stratosphere (physically linked to very cold temperatures in this region). In addition, the background static stability S is a maximum in this region (Grise et al. 2010), enhancing the temperature sensitivity to upwelling via Eq. (5). The combination of enhanced stability and long radiative damping time scale near and above the tropopause is responsible for enhanced temperature response to tropical upwelling for low frequencies (including the annual cycle) and makes this region especially sensitive to low-frequency dynamical forcing. In contrast, the coherent signals associated with the MJO produce proportionately smaller temperature variations in the lower stratosphere (and near the cold point) because of the smaller temperature sensitivity to upwelling for 30–60-day time scales.

Acknowledgments. We are grateful to Marta Abalos, Rolando Garcia, Peter Hitchcock, Alison Ming, Alan Plumb, and Mike Wallace for discussions and comments on the manuscript. Mike Wallace and two anonymous reviewers provided insightful reviews and suggestions that significantly improved the paper. This work was partially supported under the NASA *Aura* and GPS Science Team Programs.

REFERENCES

Abalos, M., W. J. Randel, and E. Serrano, 2012: Variability in upwelling across the tropical tropopause and correlations with tracers in the lower stratosphere. *Atmos. Chem. Phys.,* **12,** 11 505–11 517, doi:10.5194/acp-12-11505-2012.

——, ——, D. E. Kinnison, and E. Serrano, 2013: Quantifying tracer transport in the tropical lower stratosphere using WACCM. *Atmos. Chem. Phys.,* **13,** 10 591–10 607, doi:10.5194/acp-13-10591-2013.

——, ——, and E. Serrano, 2014: Dynamical forcing of subseasonal variability in the tropical Brewer–Dobson circulation. *J. Atmos. Sci.,* **71,** 3439–3453, doi:10.1175/JAS-D-13-0366.1.

Andrews, D. G., J. R. Holton, and C. B. Leovy, 1987: *Middle Atmosphere Dynamics.* Academic Press, 489 pp.

Anthes, R. A., and Coauthors, 2008: The COSMIC/FORMOSAT-3 mission: Early results. *Bull. Amer. Meteor. Soc.,* **89,** 313–333, doi:10.1175/BAMS-89-3-313.

Baldwin, M. P., and Coauthors, 2001: The quasi-biennial oscillation. *Rev. Geophys.,* **39,** 179–229, doi:10.1029/1999RG000073.

Birner, T., and H. Bönisch, 2011: Residual circulation trajectories and transit times into the extratropical lowermost stratosphere. *Atmos. Chem. Phys.,* **11,** 817–827, doi:10.5194/acp-11-817-2011.

Calvo, N., R. R. Garcia, W. J. Randel, and D. Marsh, 2010: Dynamical mechanism for the increase in tropical upwelling in the lowermost tropical stratosphere during warm ENSO events. *J. Atmos. Sci.,* **67,** 2331–2340, doi:10.1175/2010JAS3433.1.

Calvo Fernández, N., R. R. Garcia, R. G. Herrera, D. G. Puyol, L. G. Presa, E. H. Martin, and P. R. Rodiguez, 2004: Analysis of the ENSO signal in tropospheric and stratospheric temperatures observed by MSU, 1979–2000. *J. Climate,* **17,** 3934–3946, doi:10.1175/1520-0442(2004)017<3934:AOTESI>2.0.CO;2.

Davis, S. M., C. K. Liang, and K. H. Rosenlof, 2013: Interannual variability of tropical tropopause layer clouds. *Geophys. Res. Lett.,* **40,** 2862–2866, doi:10.1002/grl.50512.

Dee, D. P., and Coauthors, 2011: The ERA-Interim reanalysis: Configuration and performance of the data assimilation system. *Quart. J. Roy. Meteor. Soc.,* **137,** 553–597, doi:10.1002/qj.828.

Dessler, A. E., M. R. Schoeberl, T. Wang, S. M. Davis, and K. H. Rosenlof, 2013: Stratospheric water vapor feedback. *Proc. Natl. Acad. Sci. USA,* **110,** 18 087–18 091, doi:10.1073/pnas.1310344110.

Dunkerton, T. J., C.-P. F. Hsu, and M. E. McIntyre, 1981: Some Eulerian and Lagrangian diagnostics for a model stratospheric warming. *J. Atmos. Sci.,* **38,** 819–843, doi:10.1175/1520-0469(1981)038<0819:SEALDF>2.0.CO;2.

Fueglistaler, S., P. H. Haynes, and P. M. Forster, 2011: The annual cycle in lower stratospheric temperatures revisited. *Atmos. Chem. Phys.,* **11,** 3701–3711, doi:10.5194/acp-11-3701-2011.

——, and Coauthors, 2013: The relation between atmospheric humidity and temperature trends for stratospheric water. *J. Geophys. Res. Atmos.,* **118,** 1052–1074, doi:10.1002/jgrd.50157.

Garcia, R. R., 1987: On the mean meridional circulation of the middle atmosphere. *J. Atmos. Sci.,* **44,** 3599–3609, doi:10.1175/1520-0469(1987)044<3599:OTMMCO>2.0.CO;2.

Gómez-Escolar, M., N. Calvo, D. Barriopedro, and S. Fueglistaler, 2014: Tropical response to stratospheric sudden warmings and

its modulation by the QBO. *J. Geophys. Res. Atmos.,* **119,** 7382–7395, doi:10.1002/2013JD020560.

Grise, K. M., and D. W. J. Thompson, 2012: Equatorial planetary waves and their signature in atmospheric variability. *J. Atmos. Sci.,* **69,** 857–874, doi:10.1175/JAS-D-11-0123.1.

——, and ——, 2013: On the signatures of equatorial and extratropical wave forcing in tropical tropopause layer temperatures. *J. Atmos. Sci.,* **70,** 1084–1102, doi:10.1175/JAS-D-12-0163.1.

——, ——, and T. Birner, 2010: A global survey of static stability in the stratosphere and upper troposphere. *J. Climate,* **23,** 2275–2292, doi:10.1175/2009JCLI3369.1.

Hartmann, D. E., J. R. Holton, and Q. Fu, 2001: The heat balance of the tropical tropopause, cirrus and stratospheric dehydration. *Geophys. Res. Lett.,* **28,** 1969–1972, doi:10.1029/2000GL012833.

Hitchcock, P., T. G. Shepherd, and S. Yoden, 2010: On the approximation of local and linear radiative damping in the middle atmosphere. *J. Atmos. Sci.,* **67,** 2070–2085, doi:10.1175/2009JAS3286.1.

Jenkins, G. M., and D. G. Watts, 1968: *Spectral Analysis and Its Applications.* Holden-Day, 525 pp.

Kim, J., and S.-W. Son, 2012: Tropical cold-point tropopause: Climatology, seasonal cycle, and intraseasonal variability derived from COSMIC GPS radio occultation measurements. *J. Climate,* **25,** 5343–5360, doi:10.1175/JCLI-D-11-00554.1.

——, K. M. Grise, and S.-W. Son, 2013: Thermal characteristics of the cold-point tropopause region in CMIP5 models. *J. Geophys. Res. Atmos.,* **118,** 8827–8841, doi:10.1002/jgrd.50649.

Li, Y., and D. W. J. Thompson, 2013: The signature of the stratospheric Brewer–Dobson circulation in tropospheric clouds. *J. Geophys. Res. Atmos.,* **118,** 3486–3494, doi:10.1002/jgrd.50339.

Manney, G. L., and Coauthors, 2009: Aura Microwave Limb Sounder observations of dynamics and transport during the record-breaking 2009 Arctic stratospheric major warming. *Geophys. Res. Lett.,* **36,** L12815, doi:10.1029/2009GL038586.

——, and Coauthors, 2011: Unprecedented Arctic ozone loss in 2011. *Nature,* **478,** 469–475, doi:10.1038/nature10556.

Mote, P. W., and Coauthors, 1996: An atmospheric tape recorder: The imprint of tropical tropopause temperatures on stratospheric water vapor. *J. Geophys. Res.,* **101,** 3989–4006, doi:10.1029/95JD03422.

Munchak, L. A., and L. L. Pan, 2014: Separation of the lapse rate and the cold point tropopauses in the tropics and the resulting impact on cloud top-tropopause relationships. *J. Geophys. Res. Atmos.,* **119,** 7963–7978, doi:10.1002/2013JD021189.

Newman, P. A., and E. R. Nash, 2005: The unusual Southern Hemisphere stratosphere winter of 2002. *J. Atmos. Sci.,* **62,** 614–628, doi:10.1175/JAS-3323.1.

Norton, W. A., 2006: Tropical wave driving of the annual cycle in tropical tropopause temperatures. Part II: Model results. *J. Atmos. Sci.,* **63,** 1420–1431, doi:10.1175/JAS3698.1.

Plumb, R. A., 2002: Stratospheric transport. *J. Meteor. Soc. Japan,* **80,** 793–809.

Randel, W. J., 1993: Global variations of zonal mean ozone during stratospheric warming events. *J. Atmos. Sci.,* **50,** 3308–3321, doi:10.1175/1520-0469(1993)050<3308:GVOZMO>2.0.CO;2.

——, and E. J. Jensen, 2013: Physical processes in the tropical tropopause layer and their role in a changing climate. *Nat. Geosci.,* **6,** 169–176, doi:10.1038/ngeo1733.

——, R. R. Garcia, and F. Wu, 2002: Time dependent upwelling in the tropical lower stratosphere estimated from the zonal-mean momentum budget. *J. Atmos. Sci.,* **59,** 2141–2152, doi:10.1175/1520-0469(2002)059<2141:TDUITT>2.0.CO;2.

——, F. Wu, and W. Rivera Rios, 2003: Thermal variability of the tropical tropopause region derived from GPS/MET observations. *J. Geophys. Res.,* **108,** 4024, doi:10.1029/2002JD002595.

——, R. R. Garcia, N. Calvo, and D. Marsh, 2009: ENSO influence on zonal mean temperature and ozone in the tropical lower stratosphere. *Geophys. Res. Lett.,* **36,** L15822, doi:10.1029/2009GL039343.

Sato, K., F. Hasegawa, and I. Hirota, 1994: Short-period disturbances in the equatorial lower stratosphere. *J. Meteor. Soc. Japan,* **72,** 859–872.

Scherllin-Pirscher, B., C. Deser, S.-P. Ho, C. Chou, W. Randel, and Y.-H. Kuo, 2012: The vertical and spatial structure of ENSO in the upper troposphere and lower stratosphere from GPS radio occultation measurements. *Geophys. Res. Lett.,* **39,** L20801, doi:10.1029/2012GL053071.

Seidel, D. J., R. J. Ross, J. K. Angell, and G. C. Reid, 2001: Climatological characteristics of the tropical tropopause as revealed by radiosondes. *J. Geophys. Res.,* **106,** 7857–7878, doi:10.1029/2000JD900837.

Simpson, I. R., T. G. Shepherd, and M. Sigmond, 2011: Dynamics of the lower stratospheric circulation response to ENSO. *J. Atmos. Sci.,* **68,** 2537–2566, doi:10.1175/JAS-D-11-05.1.

Ueyama, R., and M. J. Wallace, 2010: To what extent does high-latitude wave forcing drive tropical upwelling in the Brewer–Dobson circulation? *J. Atmos. Sci.,* **67,** 1232–1246, doi:10.1175/2009JAS3216.1.

——, E. P. Gerber, J. M. Wallace, and D. M. W. Frierson, 2013: The role of high-latitude waves in the intraseasonal to seasonal variability of tropical upwelling in the Brewer–Dobson circulation. *J. Atmos. Sci.,* **70,** 1631–1648, doi:10.1175/JAS-D-12-0174.1.

Virts, K. S., and J. M. Wallace, 2014: Observations of temperature, wind, cirrus, and trace gases in the tropical tropopause transition layer during the MJO. *J. Atmos. Sci.,* **71,** 1143–1157, doi:10.1175/JAS-D-13-0178.1.

Wallace, J. M., R. L. Panetta, and J. Estberg, 1993: Representation of the equatorial stratospheric quasi-biennial oscillation in EOF phase space. *J. Atmos. Sci.,* **50,** 1751–1762, doi:10.1175/1520-0469(1993)050<1751:ROTESQ>2.0.CO;2.

Wang, J. S., D. J. Seidel, and M. Free, 2012: How well do we know recent climate trends at the tropical tropopause? *J. Geophys. Res.,* **117,** D09118, doi:10.1029/2012JD017444.

Wickert, J., and Coauthors, 2001: Atmosphere sounding by GPS radio occultation: First results from CHAMP. *Geophys. Res. Lett.,* **28,** 3263–3266, doi:10.1029/2001GL013117.

Yulaeva, E., and J. M. Wallace, 1994: The signature of ENSO in global temperature fields derived from the Microwave Sounding Unit. *J. Climate,* **17,** 1719–1736, doi:10.1175/1520-0442(1994)007<1719:TSOEIG>2.0.CO;2.

——, J. R. Holton, and J. M. Wallace, 1994: On the cause of the annual cycle in tropical lower-stratospheric temperature. *J. Atmos. Sci.,* **51,** 169–174, doi:10.1175/1520-0469(1994)051<0169:OTCOTA>2.0.CO;2.